A study on the erosion-corrosion behaviour of engineering materials used in the geothermal industry

F. Brownlie[a,b*], T. Hodgkiess[b], A. Pearson[c], A. M. Galloway[a]

[a] *Department of Mechanical & Aerospace Engineering, University of Strathclyde, Glasgow, UK.*

[b] *Weir Advanced Research Centre, Glasgow, UK.*

[c] *Ascott Metallurgical Ltd, Glasgow, UK*

[*] *Corresponding author. E-mail address: f.brownlie@strath.ac.uk (F. Brownlie).*

Abstract

Erosion-corrosion can be a significant issue for engineering components used in the geothermal industry. This study assesses the erosion-corrosion behaviour of a wide range of engineering alloys which are used in various parts of geothermal power plants. The evaluated materials comprised a carbon steel, low-alloy steel, three grades of stainless steel together with Ni-Cr alloy (Inconel 625) and Ti-6Al-4V. Tests were conducted by utilising a submerged 90 ° impinging slurry jet consisting of silica sand particles suspended in an acidic (pH 4) aqueous solution consisting of 3.5% NaCl. Gravimetric mass losses, in-situ potentiodynamic polarisation scans and an enhanced volumetric analysis technique were used to assess the influence of hydrodynamic conditions on the erosion-corrosion behaviour of the test materials. The effect of applied cathodic protection was also examined. Post-test metallurgical examination was also conducted via SEM. The results showed the distinct differences between low alloy steels and "corrosion resistant" alloys – with the former demonstrating substantial material loss in the low-angle corrosive wear region due to large amounts of corrosion-related damage. Both superaustenitic stainless steel (UNS S31254) and Inconel 625 (UNS N06625) exhibited the greatest erosion-corrosion resistance of the test materials – with Inconel 625 demonstrating the greatest resistance to high angle corrosive wear. The relevance of the findings to materials selection and other methods of protection against surface degradation in geothermal power plants is discussed.

Keywords: erosion-corrosion, geothermal, electrochemistry

1. Introduction

Corrosion and erosion-corrosion can be a major issue for components used in geothermal power plants because geothermal systems can contain numerous aggressive constituents such as salt brines and hydrogen chloride, hydrogen sulphide and carbon dioxide gas from volcanic systems. Corrosion and erosion-corrosion in geothermal systems is dependent upon a number of operational factors including pressure, temperature, flow rate, chloride content and pH [1–3]. Just to mention two

examples, the temperatures, encountered in the geothermal fluid exiting the well, cover an extremely wide range from 65 °C to over 200 °C [4–6] and the chloride concentrations at the same point can vary from almost drinking water quality to around 20% [7]. Moreover, as they pass through the various parts of a typical geothermal plant, there are substantial changes in the temperature (hardly above ambient in some equipment items [8]) and in fluid chemistries – e.g. increase in salinity and in non-condensable gas loading respectively in the liquid and vapour exiting flashing separators. Geothermal fluids can also contain low-solubility minerals, such as silica, which can precipitate from the liquid and cause erosion issues. Corrosion and erosion-corrosion lead to operational problems including damage to geothermal turbines and other components, such as pipes, valves, pump impellers/casings and heat exchanger tubes. Many of these component parts of a geothermal system employ equipment that is common to many other engineering activities – but, often, in more challenging conditions which can lead to high costs associated with maintenance, materials and loss of power production.

Carbon- and low-alloy steels are widely used in the geothermal industry for pipelines, casings and tubing [9]. In neutral-pH and moderately saline environments (94-1500ppm Cl^-), carbon- and low-alloy steels are generally observed to be satisfactory [9] and erosion-corrosion rates can be comparable with stainless steels [10]. However, in low-pH conditions (pH 2-4) the corrosion rate can be as high as 322mm/yr in some geothermal environments [11]. Scaling has also been observed to be an issue, which can cause a number of operational problems and also has hindered some in-situ experimental testing at geothermal sites [6,12].

Stainless steels are also used for a variety of components within geothermal industry, including valves, turbine components and heat exchanger tubes. An austenitic (UNS S31603) and a duplex (UNS S31803) stainless steel have shown good resistance to general surface and pitting corrosion in flowing artificial geothermal water of low salinity and alkaline pH at 150 °C [13]. In simulated geothermal environments of high salinity, however, even the superduplex and superaustenitic grades of stainless steel have been observed to be vulnerable to pitting and crevice corrosion [14]. Much more attention has been devoted to the investigation of corrosion behaviour – as opposed to erosion-corrosion of stainless steels in geothermal environments [9] but, under in-situ geothermal environmental testing, stainless steel (UNS S31254 and UNS S32707) pipework and bends have been observed to experience localised regions of corrosion pitting and erosion damage [6].

Due to their generally good corrosion resistance at high temperature, Ni-Cr alloys have seen application for components within geothermal power plants. Studies of a number of nickel-base alloys have demonstrated this aspect. For instance, UNS N06059 (Ni- 22Cr, 14Mo) was observed to possess good resistance to pitting attack in highly-saline simulated geothermal fluid at 150 °C [14]. Other work

[15] has shown that UNS N66250 (Ni-20Cr-8Mo-5Fe) has a high degree of uniform corrosion resistance (0.01-0.02 mm/yr) in geothermal brine at 250 °C and a pH range of 4.6-4.8 with a chloride content ranging from 1 wt.%-20 wt.%. Another report [16] claims that nickel alloys with a chromium content greater than 15 wt.% substantially lowered the corrosion rate of nickel-based alloys and that UNS N66250 and UNS N10276 (Ni-14.5Cr-15Mo-4Fe) demonstrated the greatest tendency, of Ni-Cr alloys, for passivity when exposed to geothermal brines.

Titanium alloys have also been employed for geothermal components [9], such as well tubulars [17], due to their general good corrosion resistance to brine and acidic environments. Titanium alloys (UNS R52400 – Ti-0.3Fe-0.25O-0.12Pd, UNS R53400 – Ti-0.6Ni-0.3Fe-0.2Mo, UNS R56400 – Ti-6Al-4V) have been observed to have good uniform corrosion resistance under geothermal brines (200-300 °C, pH 2-4, chloride content up to 129,000 ppm) [18,19], however, they have been observed to be vulnerable to localised corrosion [18].

It is very evident that numerous investigations, of the *corrosion* behaviour of candidate materials in geothermal systems, have been undertaken. In contrast, detailed consideration of erosion corrosion, in controlled conditions, has received scant attention hitherto. Even reports that mention this phenomenon (sometimes in the title) often do not include any detailed results or discussion. A few investigators have considered the influence of flow on corrosion but the detailed study of the effect of the presence of suspended solids is virtually absent. One reason behind the dearth of in-situ monitoring of erosion corrosion, is the issue of scaling which has been observed in several studies [4,6,12] to complicate the assessment of in-situ experimental erosion-corrosion studies.

It is obvious that the progress of erosion-corrosion will be affected by factors such as flow velocity, solids loading, temperature and chemical constitution of the fluid. In the general field of erosion-corrosion research, demonstrations of these features have been produced: effect of increasing temperature [20], flow velocity [21], solid loading [22]. It has also been widely shown that the magnitude of erosion-corrosion damage involves contributions from pure mechanical, pure corrosion and complex interactive phenomena. It is evident that quite different corrosive environments such as, for example, aerated saline water [23–26] typical of marine conditions and carbon-dioxide-containing fluids found in oil/gas transportation pipelines [27,28], have generally similar qualitative influences on the damage. On account of the wide range of materials employed and environments experienced in geothermal power plants, it was decided to adopt one standard set of test conditions to obtain an initial, comparative measure of the erosion-corrosion behaviour of a number of candidate alloys. This experimental condition was chosen to represent a corrosive environment (acidic,

aerated, saline water) to mimic the likely influences of corrosion with a fixed amount of solids and constant temperature.

The erosion-corrosion tests are conducted in a submerged, re-circulating, impinging-slurry jet test rig. Material damage is quantified by gravimetric measurements, in-situ potentiodynamic polarisation scans and via an in-house developed volumetric analysis technique [23]. Post-test SEM examination is also conducted in order to understand the corrosive wear mechanisms occurring on the test materials. Additionally, the influence of applied cathodic protection was examined.

2. Materials & methods

The materials assessed in this study are summarised in Table 1 including typical applications in geothermal systems. The nominal compositions and hardness of the studied materials are given in Table 2 and 3 respectively.

Table 1: *List of test materials along with their designation and typical applications in geothermal systems*

Alloy	Designation	Typical applications in Geothermal systems
Carbon steel	EN10028:2 P265GH	Pipelines
Low alloy steel	ASTM A470 Grade C	Turbine rotor components
Precipitation hardened stainless steel	UNS S17400	Valve stems and turbine components
Austenitic stainless steel	UNS S30403	Turbine blades
Superaustenitic stainless steel	UNS S31254	Heat exchanger tubes.
Ni-Cr superalloy	UNS N66250	Pump components
alpha-beta titanium alloy	UNS R56400	Pump components

Table 2: *Nominal chemical composition (%wt.) for the tested materials*

Test Material	C	Mn	Si	Cr	Ni	Fe	Ti	Al	Mo	V
P265GH	0.2	0.6-1.2	0.35	0.3	0.3	Bal.	0.03	0.02	0.08	0.02
UNS S17400	0.07	1	1	15-17.5	3-5	Bal.	-	-	-	-
ASTM A470 Grade C	0.2-0.35	0.1	0.12	0.8-2.0	1.5-6.5	Bal.	-	0.01	0.9-2.0	0.2-0.4
UNS S30403	0.035	2	1	18-20	8-12	Bal.	-	-	-	-

UNS R56400	0.1	-	-	-	-	0.3	Bal.	6	-	4
UNS N66250	0.1	0.5	0.5	20-23	Bal.	5	0.4	0.4	-	-
UNS S31254	≤0.02	≤1.0	≤0.8	20	18	Bal.	-	-	6.1	-

Table 3: *Nominal hardness values for the tested materials*

Test material	P265GH	UNS S17400	ASTM A470 Grade C	UNS S30403	UNS R56400	UNS N66250	UNS S31254
Hardness (HV)	332	365	340	200	320	247	227

The erosion-corrosion experiments were conducted in a recirculating, submerged, impinging-slurry test rig, as shown in Figure 1 [24]. The solid-liquid 90 ° impingement testing was conducted with a 3.5 % NaCl, pH 4 aqueous solution with 400 µm angular sand particles and a sand concentration of 0.68 g/l. The submerged jet had a velocity of 18 m/s and the nozzle diameter was 4 mm. The offset distance between the nozzle and the test specimen, S, was kept constant at 5 mm. The temperature of the aqueous solution was 40±1 °C for the full one-hour test duration. Solid-liquid impingement tests were also conducted under cathodic protection conditions in order to provide information on the material degradation mechanisms occurring on the tested materials. The application of cathodic protection was facilitated using a standard potentiostatic circuit involving an auxiliary electrode, A, and a Ag/AgCl reference electrode, R.

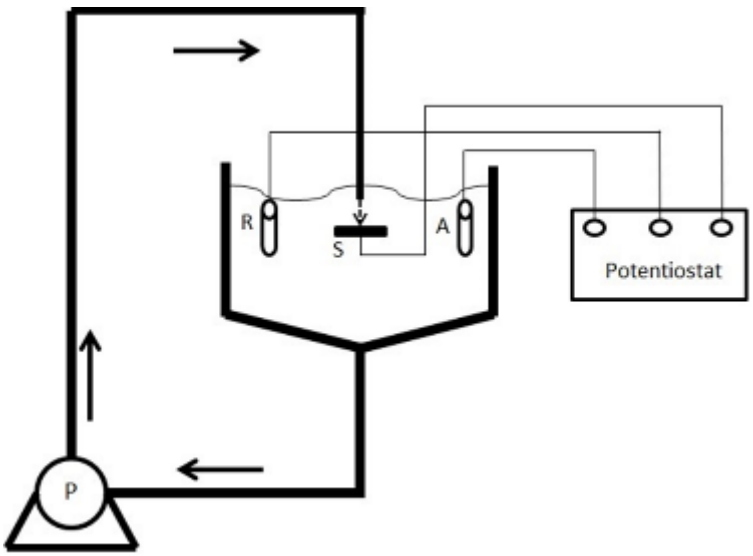

Figure 1: *Schematic diagram of the recirculating submerged impingement test rig with potentiostat*

All specimens were ground to 1200 grit SiC paper prior to testing. Gravimetric measurements were obtained before and after testing with a mass balance with an accuracy of ±0.1 mg. Mass losses were converted to volume losses via the test materials' densities. In order to provide information relating to the attack on the two main hydrodynamic regions (directly impinged and surrounding zone) of the specimen, surface topography was conducted on post-test surfaces by using a non-contact optical 3D imaging system (Alicona InfiniteFocus) with a wear scar volume accuracy of ±0.02 mm^3. Post-test surface images were obtained by using a Hitachi SU-6600 SEM with a 20 kV accelerating voltage.

Potentiodynamic polarisation scans were conducted to measure the in-situ corrosion rates of the test materials during solid-liquid impingement conditions. The potentiodynamic polarisation scans were conducted 15 minutes after the sample was submerged to allow for the free corrosion potential, E_{corr}, to stabilise. A Gill AC electrochemical monitoring equipment was utilised for the potentiodynamic polarisation and cathodic protection tests. Platinum was used as the auxiliary electrode and Ag/AgCl was used as the reference electrode. Polarisation tests were conducted by shifting the initial electrode potential either 20 mV more positive (cathodic) or 20 mV more negative (anodic) than E_{corr}, hence ensuring that the transition point would occur. Scans were then made 300 mV more negative (for cathodic scans) or 300 mV more positive (for anodic scans) at a sweep rate of 15 mV/min. The chosen ranges were sufficient to evaluate corrosion current density measurements by way of Tafel extrapolation. The measured corrosion current densities were then used to evaluate the associated volume losses from corrosion via calculation by Faraday's Law. To conduct the polarisation tests, an electrically conductive wire was connected to the rear of the specimens, which were then cold mounted in epoxy resin. For cathodic protection experiments, the electrode potential was maintained at -800 mV (Ag/AgCl) at which potential back extrapolation of the anodic polarisation curves demonstrated that residual anodic reaction rates were negligible.

3. Results & Discussion

3.1 Total volume loss

Figure 2 displays the total volume loss measurements for all the test materials under free erosion-corrosion (FEC) and cathodic protection (CP) conditions. The error bands represent the experimental scatter of at least two experiments. Under FEC conditions, the two different categories of materials – poor corrosion resistant alloys and corrosion-resistant alloys (CRAs) – performed noticeably differently. The low-alloyed steel ASTM A470 Grade C, in FEC conditions, demonstrated a volume loss almost twice as great as P265GH steel which in turn exhibited a volume loss almost three times as great as the CRAs. The Ti-based alloy, UNS R56400, and the martensitic precipitation hardened stainless steel, UNS S17400, showed the greatest volume loss of the CRAs – with the superaustenitic

stainless steel, UNS S31254, and the Ni-Cr alloy, UNS N66250, exhibiting the lowest volume loss of the test materials. However, when CP was applied, both low alloy steels exhibited similar volume losses as the CRAs and in some cases outperformed the CRAs. This finding highlights the major contribution of corrosion-related damage mechanisms to the low alloy steels during FEC conditions, as has been observed in previous studies [23,25,29–31].

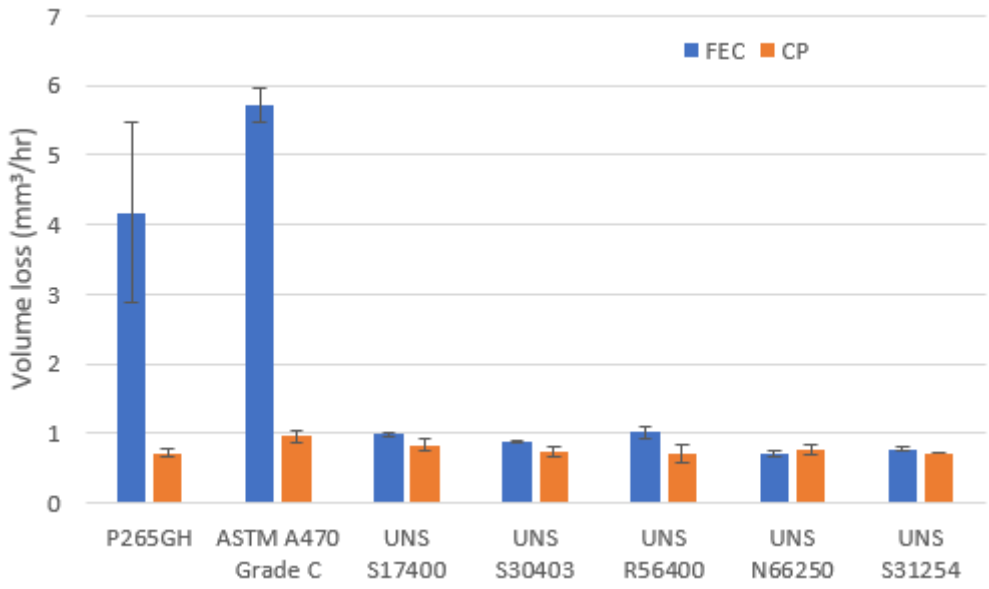

Figure 2: *Total volume losses of the tested materials under FEC and CP conditions*

3.2 Electrochemical monitoring

Figure 3 shows the potentiodynamic polarisation scans for the tested materials which were obtained during solid-liquid impingement conditions. The electrode potential has been normalised to zero volts in order to facilitate an easier comparison of the various polarisation curves. Oscillations in current density were observed from the anodic polarisation curves for the CRAs indicating de-passivation/re-passivation events. The oscillations are also evident in the initial stages of the cathodic polarisation curves. This behaviour is associated with the impacting solid particles and accompanying electrochemical transients associated with cyclic formation and breakdown of the passive film occurring over the wear regions [23,24,26].

The anodic polarisation scans also show that the both the precipitation hardened martensitic stainless, UNS S17400, and the austenitic stainless steel (UNS S30403) overlap one another as does the superaustenitic stainless steel, UNS S31254 and the titanium alloy – UNS R56400. The Ni-Cr alloy, UNS N66250, demonstrates the lowest current density values until approximately 200 mV positive to E_{corr}, at which there is an increase in current density which may be associated with passive film breakdown. Unsurprisingly, the low-alloy steels exhibit active corrosion behaviour several orders of magnitude greater than the passive alloys. For the cathodic polarisation scans, the titanium-based alloy, UNS

R56400, is demonstrating the highest current densities of the passive alloys followed closely by the austenitic stainless steel. Both of these alloys along with the precipitation hardened stainless steel and low-alloy steels, demonstrate concentration polarisation at approximately 150-250 mV negative to E_{corr}. The Ni-Cr alloy showed the lowest current densities during the entire cathodic polarisation scan.

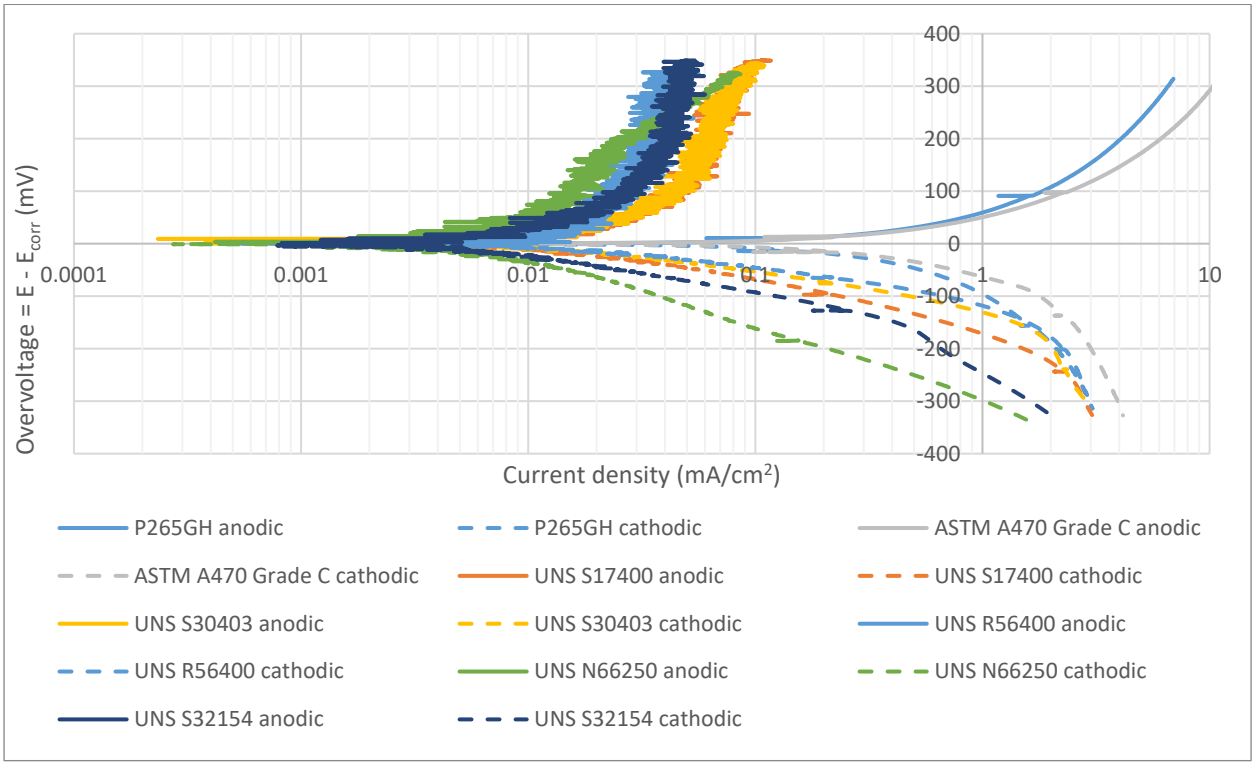

Figure 3: *Anodic and cathodic potentiodynamic polarisation scans for the tested materials*

Table 4 shows the measured free corrosion potentials (E_{corr}), corrosion current densities (i_{corr}) and calculated volume losses due to corrosion for the tested materials. For the passive alloys the volume loss due to corrosion is relatively small. Both the precipitation hardened and the austenitic stainless steel exhibit similar corrosion rates, which were the greatest of the passive alloys. This is to be expected due to their lower alloying content. The superaustenitic stainless steel and the Ni-Cr alloy both demonstrated the lowest corrosion rates consistent with their high alloying content, particularly of chromium and molybdenum, hence producing the most stable passive films. As observed from the potentiodynamic polarisation scans (Figure 3), both low-alloy steels exhibit the highest corrosion rates, several orders of magnitude greater than those of the passive alloys.

Table 4: *Free corrosion potential, corrosion current densities and volume losses due to corrosion (calculated by Faraday's Law) for the tested materials*

Material	E_{corr} (mV)	i_{corr} (mA/cm^2)	Volume loss (mm^3/hr)

P265GH	-494	0.55	1.28
ASTM A470 Grade C	-472	0.8	1.21
UNS S17400	-460	0.021	0.031
UNS S30403	-464	0.023	0.033
UNS R56400	-444	0.017	0.019
UNS N06625	-331	0.007	0.012
UNS S31254	-459	0.009	0.011

3.3 Breakdown of wear mechanisms

The contribution of the various materials degradation mechanisms, associated with erosion-corrosion, to the total volume loss, T, is the measured material loss under free erosion-corrosion conditions given in Equation 1.

$$T = E + C + S \quad (1)$$

Figure 4 reveals the breakdown of the wear mechanisms in terms of erosion (E) - determined by measuring weight losses under CP conditions, corrosion (C) - measured from in-situ electrochemical monitoring during solid-liquid impingement and synergy (S) which represents the influence of corrosion on erosion damage and is calculated from Equation 1, for the tested materials. For the passive alloys, the predominant wear mechanism was observed to be erosion. The martensitic precipitation hardened stainless steel was observed to have the greatest volume loss due to erosion. The lower erosion damage observed for the austenitic-based stainless steels is likely to be associated with the strain hardening effects which have been observed in previous studies [32,33]. The titanium-base, Ni-Cr alloys and austenitic stainless steels exhibit similar volume losses due to erosion. The volume loss due to corrosion for the passive alloys contributed to very small amounts of the overall material loss.

It is interesting to note that the contributions to overall damage from corrosion-related phenomena for the two low-alloyed steels are dominated by synergies which are significantly higher than their pure corrosion rates. This is a vivid example of the role of interactions between corrosion and wear during erosion corrosion. Even for the CRAs, the damage due to synergy exceeds that for pure corrosion – although the absolute magnitudes are much lower than for the carbon- and low-alloy steels. Amongst the higher-grade materials, the titanium-base alloy and the superaustenitic stainless steel demonstrated the highest volume losses due to synergy. The martensitic precipitation hardened and austenitic stainless steel exhibited similar volume losses due to synergy, which were approximately half of the synergy value of the titanium-base alloy and superaustentic stainless steel.

The synergy mechanisms for the tested materials are likely to be associated with micro-galvanic effects due to two or more phases which are present in all of the tested materials. Alpha and beta phases of the titanium alloy may experience galvanic effects which will lead to synergistic effects, as well as the precipitates, retained austenite and martensitic structure of the precipitation hardened stainless steel. Similar galvanic interactions have been observed on duplex stainless steels [34,35]. The strain hardening and induction of martensite of the austenitic stainless steels will also lead to a two-phase structure where galvanic interactions will occur and hence lead to a synergistic effect [36].

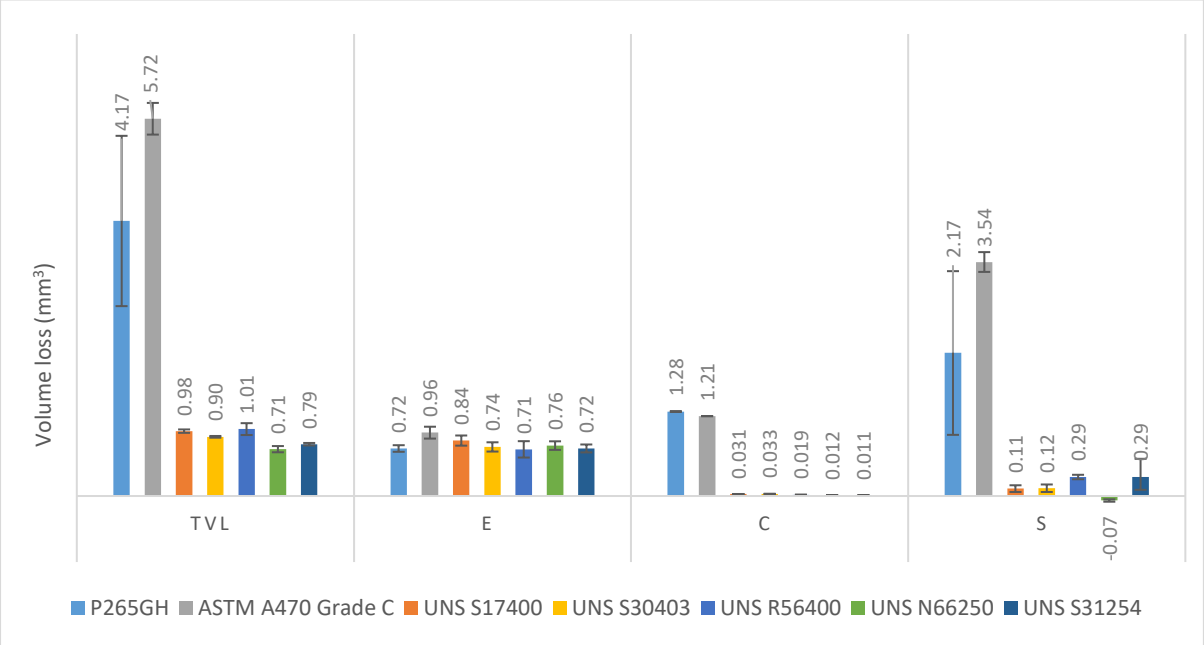

Figure 4: *Volume losses for the different wear mechanisms for the tested materials*

3.4 Post-test volumetric analysis

Post-test volumetric analysis was undertaken to assess the volume loss of the test material in the direct impinged zone. Figure 5 shows the volume loss measurement of the direct impingement zone of an ASTM A470 Grade C after a FEC test. The analysis was taken inside the region of the superimposed red ring which represents the zone directly under the impinging fluid.

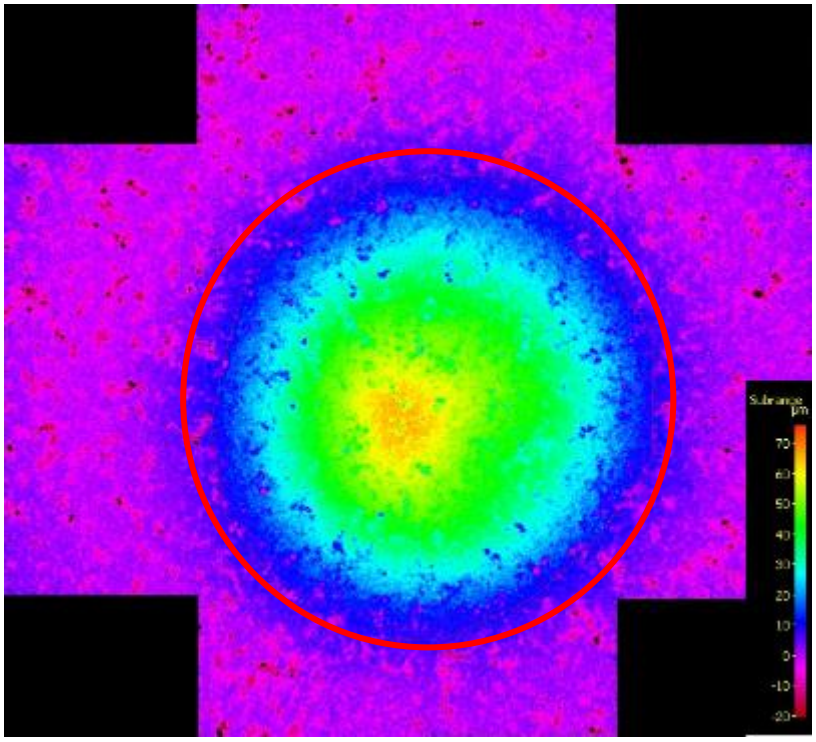

Figure 5: *Volumetric analysis of the direct impinged zone of an ASTM A470 Grade C specimen after solid-liquid impingement test*

Figures 6 and 7 summarise the volume loss measurements in the different wear regions (directly impinged zone - DIZ and outer area - OA) for the test materials under FEC and CP conditions respectively. The most evident difference between the damage in the DIZ and OA was observed for the low alloy steels (P265GH and ASTM A470 Grade C) under FEC conditions, where the volume loss measurements were significantly greater in the OA. This high volume loss can be attributed to the corrosion-related damage to which the low alloy steels are vulnerable and is expected to be more prevalent in the OA, where conditions are less erosive. However, under CP conditions, the durability of the low alloy steels is as good as, if not better, than the CRAs in both wear regions.

The Ni-Cr alloy, UNS N66250, demonstrates the greatest resistance to high-angle impingement as it has the lowest DIZ volume loss of the CRAs. However, in the OA, the superaustenitic stainless steel, UNS S31254, exhibits the greatest resistance to low angle abrasion damage, despite its relatively low hardness (227HV). This is contradictory to the typical expectation that a greater hardness will increase the abrasion resistance [37–39]. Another interesting observation of this study is that precipitation hardened stainless steel, UNS S17400, with the greatest hardness, under CP conditions, proved to possess the least resistance to high angle impingement and demonstrated poorer resistance to low angle abrasion compared to more ductile materials such as UNS S30403 and UNS S31245. An explanation for this observed behaviour, may be associated with the work hardening effects which are likely to be occurring in the austenitic-based alloys [32,33].

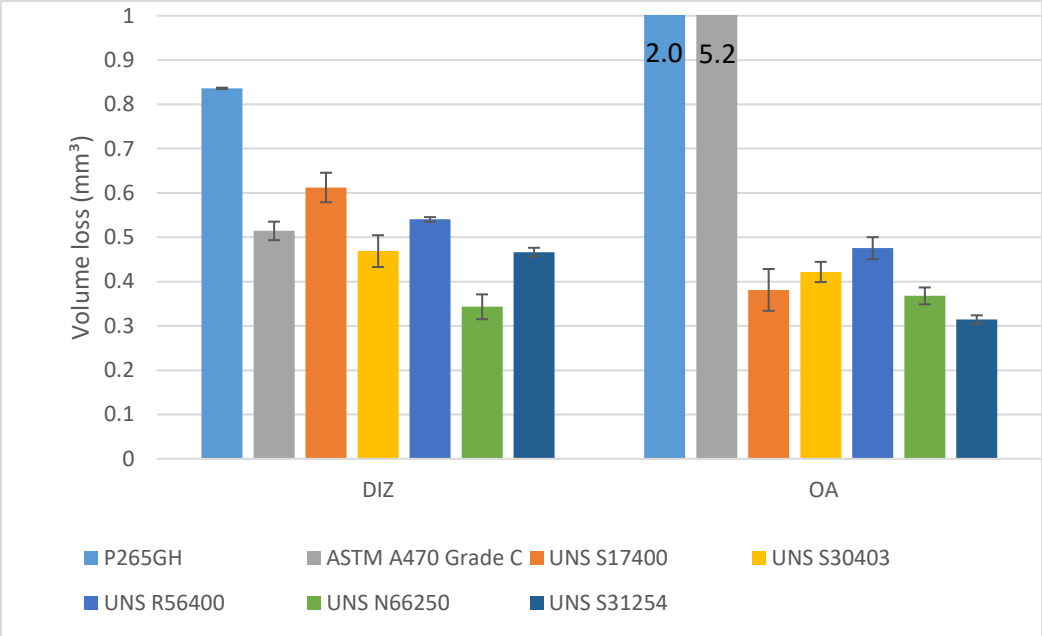

Figure 6: *Volume loss measurements in the different wear regions for the test materials under FEC conditions*

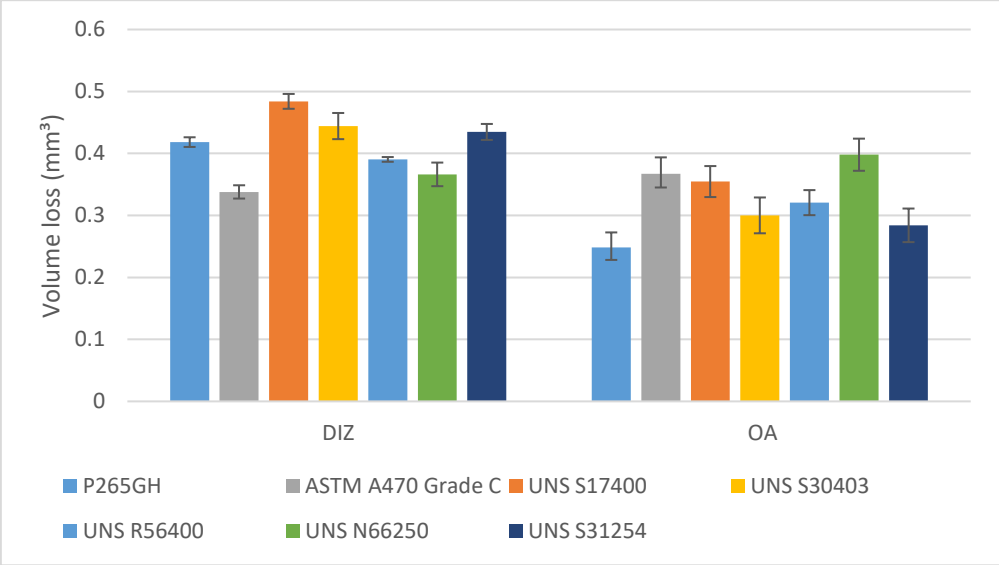

Figure 7: *Volume loss measurements in the different wear regions for the test materials under CP conditions*

3.5 Post-test microscopy

Post-test examination of specimens on the SEM, revealed very similar damage patterns on all of the investigated materials. In the directly-impinged zone, after both FEC and CP experiments, (Figures 8a and b), the sand particles have resulted in the formation of small impact craters caused by their direct impact on the material surface. The impacting sand particles cause plastic deformation of the ductile

metallic surface; where the surface is indented at high impact angle, material is smeared to the lip of the impact crater. Continuing impacts have caused the surface to roughen due to the repeated plastic deformation and smearing of the ductile metallic material. Subsequently, the thin smeared material can be easily removed by the impacting sand particles [40,41].

In the outer region, (Figures 9a and b), sliding abrasion damage marks are apparent, caused by sand particles moving along the surface the test surface at low angles. This results in a cutting-type mechanism on the soft/ductile metallic material which causes it to plastically deform and smear in the direction of the flow of the impacting sand particles [24,30]. One distinct additional feature evident (Figure 10) on the low-alloy steel, (and carbon steel) was the presence of corrosion pits.

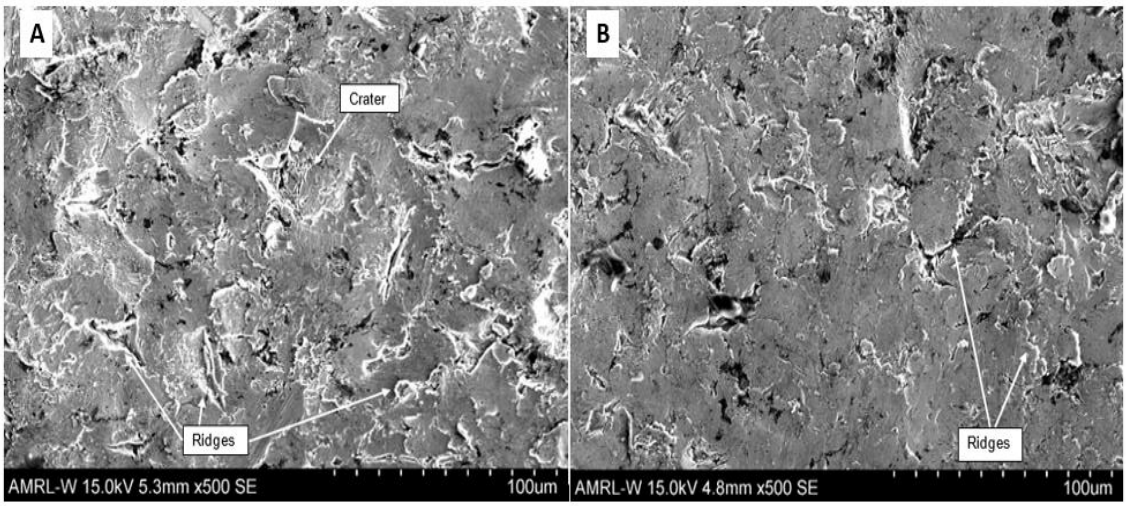

Figure 8: *A - DIZ of UNS S31254 after FEC; B - DIZ of UNS N06625 after CP*

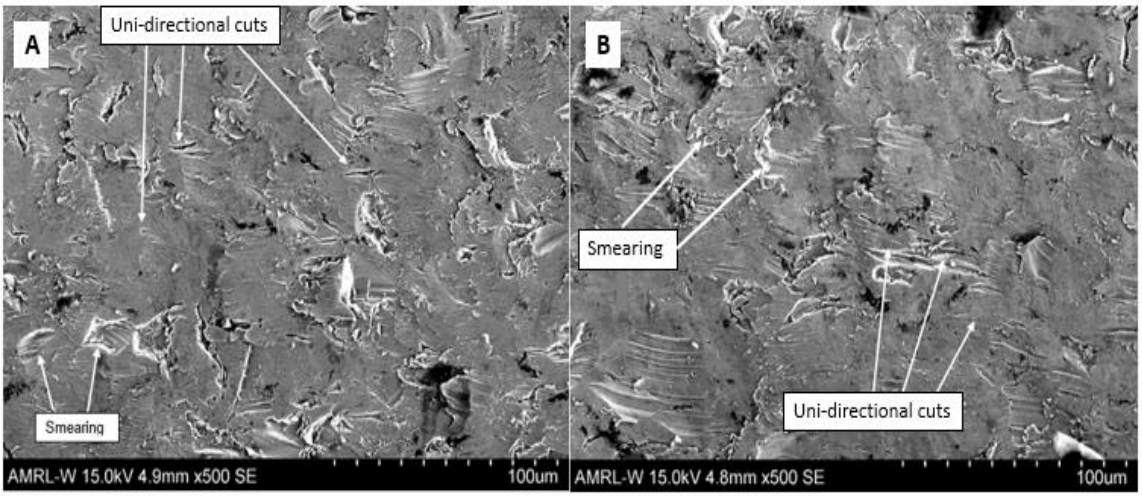

Figure 9: *A - OA of UNS S31254 after FEC; B - OA of UNS N06625 after CP*

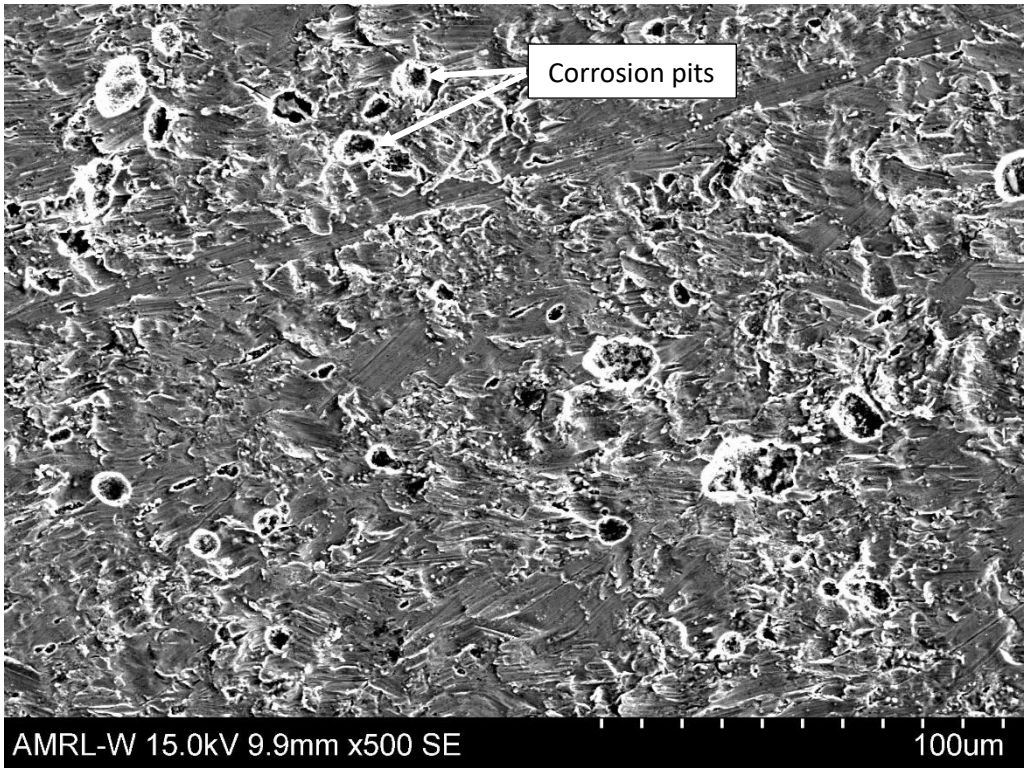

Figure 10: *ASTM A470 Grade C OA after FEC*

3.6 Relevance of findings to geothermal systems

The observations on single-sized specimens indicate that the carbon steel (P265GH) and the low-alloy steel (ASTM A470 Grade C) are extremely vulnerable in erosion-corrosion conditions in this (solids-containing) aerated, acidic, saline environment and therefore would not be applicable for use in any part of a geothermal plant in which such conditions prevail. The study has thrown light, though, on some interesting details of the behaviour:-

- The use of the method of separating the experimental data into the two distinct hydrodynamic zones (DIZ and OA) demonstrates clearly substantial differences between the relative performances of the materials
- The relative vulnerability of the carbon- and low-alloy steels applies in low-angle corrosive wear conditions only – where there is a very substantial contribution from corrosion-enhanced synergy to the overall influence of corrosion. In directly impinging conditions, these steels are scarcely any more vulnerable than the CRAs. This is especially so for the low-alloy steel ASTM A470 Grade C.
- The findings resulting from the application of cathodic protection (CP) demonstrate the benefit accruing from strategies that eliminate the corrosion part of the overall erosion-corrosion damage. With such CP applied, the low-alloy steel, ASTM A470 Grade C, is in fact the best performing alloy under direct impingement. Moreover, cathodically-protected

carbon steel (P265GH) outperformed all the other materials. In view of these findings, there appears to be negligible benefit arising from the use of the (more expensive) CRA alloys in place of the cathodically-protected lower-alloyed steels. It would be desirable that some attention be given to the possibilities of application of CP in geothermal streams. Although the impressed current type of CP may be difficult to engineer into some of the complex geometries in the flow stream, the adoption of the simpler method of CP, that employs sacrificial anodes, would be worth considering [29].

Corrosion inhibitors are routinely employed in many types of engineering equipment – including geothermal installations [5]. The question, therefore, arises as to whether such inhibitors would be also effective in reducing the severity of damage in corrosive wear conditions. It is possible to argue that the extreme turbulence in erosive flows of water, that also contains solids in suspension (e.g. sand or scale particles), might impede the establishment of the protective inhibitor film on the metallic surfaces. This qualification has been given support by work on carbon steel in CO_2 -saturated brine [27,28] which demonstrated that

- Commercially-available *corrosion* inhibitors require an order of magnitude higher dosing rate, than is appropriate in static conditions, for them to be effective under erosion-corrosion conditions
- In the presence of suspended solids, there is a tendency for inhibitor molecules to be de-activated by adsorption on the surface of sand particles.

In situations where inhibitors are not likely to be effective in erosion-corrosion circumstances, such chemicals could be retained for use as effective corrosion-only strategies by means of incorporation of screens to filter out solid particles from the fluid stream. Another approach is to consider the use of coatings for protection against corrosion and erosion corrosion in geothermal systems and this strategy is currently receiving attention in the EU Horizon 2020 Geo-coat project (no. 764086)

In the event of the carbon- and low-alloy steels being regarded as too potentially vulnerable in some parts of the geothermal circuit, consideration of the CRAs becomes relevant. When considering the suite of experimental results in the current study (single specimen, DIZ, OA) in FEC conditions, the nickel-base alloy, (UNS N66250) exhibits the greatest resistance to material loss, this is in-line with previous work on corrosion resistance in simulated geothermal brine [14]. The super-austenitic stainless steel (UNS S32154) was found to be slightly more vulnerable compared to UNS N66250 but significantly more resistant than the other two (lower-alloyed) stainless steels.

One of the most striking features is the observation of the titanium-base alloy (UNS R56400) undergoing more extensive damage than all the other CRAs. This amounts to a material loss rate of

approximately double for the titanium alloy compared to the more resistant (Ni-Cr alloy – UNS N66250 or super-austenitic stainless steel – UNS S31254) in both direct impinging and low-angle sliding conditions. This greater vulnerability appears to be linked to the higher corrosion rates exhibited (Figure 3, Table 4) by this alloy and is also indicated by the relatively-large reduction in corrosion-related attack shown by comparing the FEC and CP results (Figure 1). This corrosion behaviour might appear to be somewhat at odds with the general notion of relatively-high corrosion resistance of titanium-base alloys. Such durability, however, is a feature of behaviour in either quiescent conditions or in flowing aqueous liquids that do not contain solid particles [42]. In the current study, the contribution of corrosion-enhanced synergy (S) to the overall material loss is a significant factor in causing the relatively-high material loss of the titanium alloy. The synergy contribution amounted to about 30% of the total material loss – a figure that is remarkably similar to that reported by McDougall and Neville [43] for the same titanium-base alloy in very similar experimental circumstances.

In summary with respect to the aspect of materials selection involving CRAs, it would appear that benefits are likely to be secured by considering the choice of the super-austenitic stainless steel rather than the lower-grade stainless steels for relevant geothermal components. This investigation, however, has provided some persuasive evidence for the consideration of the replacement of less-durable CRAs by the nickel-base alloy (UNS N66250). Interestingly, this alloy – although well known for its static corrosion resistance – does not seem to have received much attention for service in corrosive-wear situations. Finally, although this study has been focused on the potential of CRAs in geothermal equipment, many of the findings discussed above have relevance to other engineering systems that operate in moderately acidic, aerated saline environments.

4. Conclusions

- This study has focused on the largely un-researched topic of corrosive wear of candidate engineering alloys in the geothermal industry. The investigation has unravelled the detailed mechanisms involved in the overall degradation process and, hence, has facilitated a useful appreciation of the widely-different types of behaviour of such materials.
- The post-test analysis, that has been employed, has revealed substantial differences in the behaviour of some of the materials in the two distinct hydrodynamic zones (DIZ and OA).
- Carbon steel and low-alloy steel demonstrated a vulnerability to corrosion-related damage, particularly in low-angle corrosive wear situations. The effect of synergy was observed to exceed that of pure corrosion. However, when CP was applied, the lower-alloyed steels exhibited similar, and in some instances improved, resistance to both high-angle erosive wear and low-angle, abrasive-like wear, compared to the passive alloys.

- Under FEC conditions, the Ni-Cr alloy (UNS N66250) and superaustenitic stainless steel (UNS S32154) exhibited an improvement in erosion-corrosion resistance compared to the other passive alloys.
- The Ti-6Al-4V alloy was less durable, in erosion-corrosion conditions, than most of the other CRAs; this feature was related to the relative vulnerability of this alloy to corrosion-related deterioration.
- Under CP conditions, the passive alloy rankings altered depending upon the wear region. UNS N66250 was the best performing passive alloy under high-angle erosion. Whereas, UNS S32154 was the most superior of the passive alloys, under low-angle abrasive wear.

Acknowledgments

The authors would like to acknowledge the support for this study, which was provided by the Weir Group PLC (WARC2011- SAA1, 2011) via its establishment of the Weir Advanced Research Centre (WARC) at the University of Strathclyde. This work is part of the H2020 EU project Geo-Coat: "Development of novel and cost-effective corrosion resistant coatings for high temperature geothermal applications" funded by the H2020 EU project no. 764086.

References

[1] J. Nogara, S.J. Zarrouk, Corrosion in geothermal environment: Part 1: Fluids and their impact, Renew. Sustain. Energy Rev. 82 (2018) 1333–1346. https://doi.org/10.1016/j.rser.2017.06.098.

[2] O.A. Povarov, G. V Tomarov, V.E. Lusin, Erosion-Corrosion wear of Metal in Geothermal Power Plant Equipment, in: 21st New Zeal. Geotherm. Work., 1997: pp. 199–204.

[3] I. Csaki, C.A. Manea, R. Trusca, S.N. Karlsdottir, R. Stefanoiu, V. Geanta, Microstructural study on the corrosion effect on AlCrFeNiMn multicomponent alloy tested in geothermal environment, NACE Int. Corros. Expo 2017. Paper no. 8916.

[4] K.R. Ragnarsdottir, S.N. Karlsdottir, K. Leosson, A. Arnbjornsson, S. Gudlaugsson, H.O. Haraldsdottir, A. Buzaianu, I. Csaki, G. Popescu, Corrosion testing of coating materials for geothermal turbine application, NACE Int. Corros. Expo 2017. Paper no. 9185.

[5] J.G. Veldkamp, T. V Goldberg, P.M.M.C. Bressers, F. Wilschut, Corrosion in Dutch geothermal systems, TNO 2015 R10160 report, 2016.

[6] S.N. Karlsdottir, K.R. Ragnarsdottir, A. Moller, I.O. Thorbjornsson, A. Einarsson, On-site erosion-corrosion testing in superheated geothermal steam, Geothermics. 51 (2014) 170–181. https://doi.org/10.1016/j.geothermics.2014.01.007.

[7] N. Mundhenk, P. Huttenloch, B. Sanjuan, T. Kohl, H. Steger, R. Zorn, Corrosion and scaling as interrelated phenomena in an operating geothermal power plant, Corros. Sci. 70 (2013) 17–28. https://doi.org/10.1016/j.corsci.2013.01.003.

[8] S.N. Karlsdóttir, S.M. Hjaltason, K.R. Ragnarsdóttir, Corrosion behavior of materials in hydrogen sulfide abatement system at Hellisheiði geothermal power plant, Geothermics. 70 (2017) 222–229. https://doi.org/10.1016/j.geothermics.2017.06.010.

[9] J. Nogara, S.J. Zarrouk, Corrosion in geothermal environment Part 2: Metals and alloys, Renew. Sustain. Energy Rev. 82 (2018) 1347–1363. https://doi.org/10.1016/j.rser.2017.06.091.

[10] G. V. Tomarov, A.A. Shipkov, Erosion-corrosion of metals in multicomponent geothermal flows, Therm. Eng. 53 (2006) 188–194. https://doi.org/10.1134/S0040601506030049.

[11] K. Y, S. N, I. Nanjo H, K. J., Material damages in geothermal power plants, in: 14th New Zeal. Geotherm. Work., 1992.

[12] H.O. Haraldsdottir, K.R. Ragnarsdottir, S.N. Karlsdottir, D.I. Olaffson, S. Gudlaugsson, In-situ erosion-corrosion testing equipment for geothermal environment and comparative results for tested electric arc sprayed titanium, NACE Int. Corros. Expo 2019. Paper no. 13457.

[13] R. Bäßler, A. Boduch, J. Sobetzki, Corrosion resistance of high-alloyed materials in flowing artificial geothermal water, NACE Int. Corros. Expo 2014. Paper no. 3825.

[14] R. Bäßler, J. Sobetzki, H. S. Klapper, Corrosion resistance of high-alloyed materials in artificial geothermal fluids, NACE Int. Corros. Expo 2013. Paper no. 2327.

[15] D. Shannon, Corrosion of iron-base alloys versus alternate materials in geothermal brines, (Interim Report-Period Ending October 1977) [No. PNL-2456]. Richland, WA, United States: Pacific Northwest National Laboratory (PNNL); 1977.

[16] J.P. Carter, S.D. Cramer, Materials of construction for high-salinity geothermal brines, 1992. http://www.cdc.gov/niosh/nioshtic-2/10011568.html.

[17] R. Thomas, Titanium in the geothermal industry, Geothermics. 32 (2003) 679–687. https://doi.org/10.1016/j.geothermics.2003.08.004.

[18 S. Cramer, J. Carter, Corrosion in Geothermal Brines of the Salton Sea Known Geothermal Resource Area, Geotherm. Scaling Corros. (2009) 113-113–29. https://doi.org/10.1520/stp30068s.

[19] Y. Kurata, N. Sanada, H. Nanjo, J. Ikeuchi, Casing pipe materials for deep geothermal wells, [No. CONF-951037]. Davis, CA, United States: Geothermal Resources Council, 1995.

[20] S. Giddey, B. Cherry, F. Lawson, M. Forsyth, Effect of increased temperature on erosion-corrosion under turbulent conditions in bayer liquor, Corros. Sci. 40 (1998) 839–842.

[21] J.G. Liu, W.L. BaKeDaShi, Z.L. Li, Y.Z. Xu, W.R. Ji, C. Zhang, G. Cui, R.Y. Zhang, Effect of flow velocity on erosion–corrosion of 90-degree horizontal elbow, Wear. 376–377 (2017) 516–525. https://doi.org/10.1016/j.wear.2016.11.015.

[22] M. Shehadeh, M. Anany, K.M. Saqr, I. Hassan, Experimental investigation of erosion-corrosion phenomena in a steel fitting due to plain and slurry seawater flow, Int. J. Mech. Mater. Eng. 9 (2014) 1–8. https://doi.org/10.1186/s40712-014-0022-7.

[23] L. Giourntas, T. Hodgkiess, A.M. Galloway, Enhanced approach of assessing the corrosive wear of engineering materials under impingement, Wear. 338–339 (2015) 155–163. https://doi.org/10.1016/j.wear.2015.06.004.

[24] F. Brownlie, C. Anene, T. Hodgkiess, A. Pearson, A.M. Galloway, Comparison of Hot Wire TIG Stellite 6 weld cladding and lost wax cast Stellite 6 under corrosive wear conditions, Wear. 404–405 (2018). https://doi.org/10.1016/j.wear.2018.03.004.

[25] A. Neville, T. Hodgkiess, J.T. Dallas, A study of the erosion-corrosion behaviour of engineering steels for marine pumping applications, Wear. 186–187 (1995) 497–507. https://doi.org/10.1016/0043-1648(95)07145-8.

[26] S. Aribo, R. Barker, X. Hu, A. Neville, Erosion–corrosion behaviour of lean duplex stainless steels in 3.5% NaCl solution, Wear. 302 (2013) 1602–1608. https://doi.org/10.1016/j.wear.2012.12.007.

[27] J. Owen, C. Ramsey, R. Barker, A. Neville, Erosion-corrosion interactions of X65 carbon steel in aqueous CO2 environments, Wear. 414–415 (2018) 376–389. https://doi.org/10.1016/j.wear.2018.09.004.

[28] E. V. Senatore, W. Taleb, J. Owen, Y. Hua, J.A.C.P. Gomes, R. Barker, A. Neville, Evaluation of high shear inhibitor performance in CO2-containing flow-induced corrosion and erosion-corrosion environments in the presence and absence of iron carbonate films, Wear. 404–405 (2018) 143–152. https://doi.org/10.1016/j.wear.2018.03.014.

[29] F. Brownlie, L. Giourntas, T. Hodgkiess, I. Palmeira, O. Odutayo, A.M. Galloway, A. Pearson, Effect of cathodic protection methods on ferrous engineering materials under corrosive wear conditions, Corros. Eng. Sci. Technol. (2020) 1–7. https://doi.org/10.1080/1478422X.2020.1742997.

[30] L. Giourntas, T. Hodgkiess, A.M. Galloway, Comparative study of erosion–corrosion performance on a range of stainless steels, Wear. 332–333 (2015) 1051–1058. https://doi.org/10.1016/j.wear.2014.12.052.

[31] A. Neville, C. Wang, Erosion-corrosion of engineering steels-Can it be managed by use of chemicals?, Wear. 267 (2009) 2018–2026. https://doi.org/10.1016/j.wear.2009.06.041.

[32] R.J.K. Wood, J.C. Walker, T.J. Harvey, S. Wang, S.S. Rajahram, Influence of microstructure on the erosion and erosion-corrosion characteristics of 316 stainless steel, Wear. 306 (2013) 254–262. https://doi.org/10.1016/j.wear.2013.08.007.

[33] T. Singh, S.N. Tiwari, G. Sundararajan, Room temperature erosion behaviour of 304, 316 and 410 stainless steels, Wear. 145 (1991) 77–100. https://doi.org/10.1016/0043-1648(91)90240-U.

[34] J.-S. Lee, K. Fushimi, T. Nakanishi, Y. Hasegawa, Y.-S. Park, Corrosion behaviour of ferrite and austenite phases on super duplex stainless steel in a modified green-death solution, Corros. Sci. 89 (2014) 111–117. https://doi.org/10.1016/j.corsci.2014.08.014.

[35] Y.H. Yau, M.A. Streicher, Galvanic corrosion of duplex FeCr-10%Ni alloys in reducing acids, in: Galvanic Corros. ASTM STP 978, 1988: pp. 220–234.

[36] M. Matsumura, Erosion-Corrosion: An Introduction to Flow Induced Macro-Cell Corrosion, Bentham Science Publishers, 2012.

[37] A.N.J. Stevenson, I.M. Hutchings, Wear of Hardfacing While Cast Irons By Solid Particle Erosion, Wear. 186 (1995) 150–158. https://doi.org/10.1016/0043-1648(95)07184-9.

[38] R.J. Llewellyn, S.K. Yick, K.F. Dolman, Scouring erosion resistance of metallic materials used in slurry pump service, Wear. 256 (2004) 592–599. https://doi.org/10.1016/j.wear.2003.10.002.

[39] L. Giourntas, F. Brownlie, G. Karafyllias, T. Hodgkiess, A.M. Galloway, Effect of corrosion on abrasive wear in a range of materials, in: BHR Gr. - 23rd Int. Conf. Fluid Seal. 2016, 2016.

[40] I.M. Hutchings, Mechanisms of the Erosion of Metals by Solid Particles, Eros. Prev. Useful Appl. ASTM STP 664, W. F. Adler, Ed., American Society for Testing and Materials, (1979) 59-76.

[41] R. Bellman, A. Levy, Erosion mechanism in ductile metals, Wear. 70 (1981) 1–27. https://doi.org/10.1016/0043-1648(81)90268-4.

[42] T. Hodgkiess, D. Mantzavinos, Some comparisons of the erosion-corrosion behaviour of titanium and stainless steels, in: Stainl. Steel World 2005, 2005.

[43] B.A.B. Mcdougall, A. Neville, Understanding wear/corrosion interactions in tribo-corrosion of titanium and its alloys, in: NACE Int. Corros. Expo 2003, Paper no. 03265.